Influence of Current Density on Orientation-Controllable Growth and Characteristics of Electrochemically Deposited Au Films

Liu, Lintao; Zhu, Xiaoli; Wei, Shuhua; Zhang, Jing; Baklanov, Mikhail R.; Bastos da Silva Fanta, Alice; Niu, Jiebin; Xie, Changqing

Published in:
Journal of the Electrochemical Society

Link to article, DOI:
10.1149/2.0291901jes

Publication date:
2019

Document Version
Publisher's PDF, also known as Version of record

JES Focus Issue on Advances in Electrochemical Processes for Interconnect Fabrication in Integrated Circuits

Influence of Current Density on Orientation-Controllable Growth and Characteristics of Electrochemically Deposited Au Films

Lintao Liu,[1,2] Xiaoli Zhu,[2,z] Shuhua Wei,[1] Jing Zhang,[1] Mikhail R. Baklanov,[1] Alice Bastos da Silva Fanta,[3] Jiebin Niu,[2] and Changqing Xie[2]

[1] *School of Electronic and Information Engineering, North China University of Technology, Beijing 100144, People's Republic of China*
[2] *Key Laboratory of Microelectronic Devices and Integrated Technology, Institute of Microelectronics of Chinese Academy of Sciences, Beijing 100029, People's Republic of China*
[3] *DTU Danchip/Cen, Technical University of Denmark, Lyngby 2800, Denmark*

We demonstrate the controllable and preferentially <111> oriented growth of electrochemically deposited Au films in non-toxic sulfite electrolyte. To investigate the initial deposition, sub-10-nm-resolution orientation mapping of the Au thin films used as cathode was performed. On this cathode, the nucleation density and growth rate of nuclei are simultaneously modulated by tuning the pulse current density, resulting in variations in morphology, grain size and crystal orientation. These distinct textures greatly affects the characteristics of deposited Au films including Young's modulus and hardness. Furthermore, the interpretation is made for describing the formation of different microstructures in three cases. At an appropriate current density, the appropriate density of nuclei and the subsequent growth lead to preferential growth at <111> orientation and suppression of growth at other orientations. The results presented in this work would be beneficial to wide applications of Au electrochemical deposition in sulfite electrolyte.
 [DOI: 10.1149/2.0291901jes]

Manuscript submitted September 19, 2018; revised manuscript received December 4, 2018. Published December 20, 2018. *This paper is part of the JES Focus Issue on Advances in Electrochemical Processes for Interconnect Fabrication in Integrated Circuits.*

Au micro- and nanostructures with functional characteristics are widely used in both industrial applications and fundamental research including interconnections, nano-optics, nano-electronics, sensors, MEMS etc.[1–5] Electrochemical deposition is a conventional route to forming Au films and nanostructures, taking the prominent advantages of high growth rate, low cost and high fidelity of structures.[6–7] With respect to direct current electroplating, pulse electroplating (PE) is capable of modulating Au growth by adjusting depositing parameters such as peak current density, frequency and duty cycle, and thus can form Au coatings with fine grains, high uniformity and low porosity.[8–11] Additionally, among a variety of baths reported in previous studies, non-toxic sulfite baths are of great interests due to their better performance and low requirements of handling and disposal in comparison to those cyanide-based ones, which are toxic and suffer from risks in use.[12–15] To date, the modulation of the nucleation and grain growth in sulfite baths is still considered as a challenge in numerous applications such as printed circuit boards (PCB), nanolines and bottom-up filling of through silicon vias.[16–19]

Aiming to various applications of Au micro/nano structures in nano-optics and nano-electronics, theoretical studies found that the redistribution of electrons on different crystal planes of Au results in an anisotropy in the surface energy and work function, significantly affecting the interaction of Au structures with photons and electrons.[20,21] Experimental work has also shown that Au micro- and nanostuctures exibit distinct mesoscopic characteristics due to its different crystallographic morphologies.[22,23] Therefore, the crystal orientation and local textures of Au nanostructures formed by electrochemical deposition result in various electrical and optical performances. So far, the lack of knowledge on controlling preferentially oriented growth and nanotextures of Au films hampers various applications of Au electrochemical deposition, especially in environmental-friendly and non-toxic sulfite gold plating bath.

In this report, we demonstrate the modulation of nucleation and grain growth of Au films on Au seed layer in sulfite electrolyte-based electrochemical deposition by adjusting the applied current and overpotential. The preferentially <111> oriented growth of Au films can be controlled and single crystalline Au films embedded with defects are achieved on polycrystalline Au layer. These results would be helpful to a comprehensive understanding about grain growth in nanoscale and bring benefits to a wide range of applications.

Experimental

Preparation of Au films: 1), 3-nm Cr and 10-nm Au layers were evaporated as the seed layer and the cathode on a wafer. 2), 2.5 μm thick photoresist coating (S9920, Shipley, USA) was spin-coated on the seed layer (in Figure 1a) and then was exposed using an ultraviolet aligner (MA6, Karl Suss) to form a 15mm × 15mm area for electrochemical deposition (in Figure 1b). 3), Au films with thickness of 1 μm were electrochemically deposited by applying different pulse current densities in sulfite electrolyte (Elevate Gold 7990, Technic Inc) (in Figure 1c). 4), the photoresist was dissolved in acetone (in Figure 1d).

Characterization of Au seed layer: Transmission Kikuchi Diffraction (TKD) was used for characterization of crystallographic orientation of evaporated Au film. For this analysis, 5 nm Ti and 20 nm Au films were successively deposited on TEM grids having a 5 nm thick Si_3N_4 membrane (Caspilor AB, Lidingö, Sweden) using the same deposition parameters as those for the deposition on Si. The orientation maps were acquired utilizing a FEI Nova 600 NanoSEM equipped with a Bruker OPTIMUS TKD detector head. The electron beam voltage, beam current and beam step size were 30 kV, 2 nA and 3 nm, respectively. The Kikuchi diffraction patterns and grain size distributions were achieved using both CrystAlign (Bruker) and OIM TSL analysis software.

Characterization of electrochemically deposited Au films: For X-ray diffraction (XRD) analysis, the electrochemically deposited Au films were characterized using an X-ray diffractometer (SmartLab, Rigaku Corporation, Japan) equipped with a Cu Kα radiation source. The surface roughness of Au films deposited at different current densities was measured using atomic force microscope (AFM) (Dimension Icon-PT system, Bruker Corporation, Billerica, MA, USA) at the contact mode. To investigate the preferentially oriented growth of Au grains, TEM bright field images have been acquired at a 200 kV operating voltage (FEI Tecnai T20 G2 TEM, FEI Company, Hillsboro OR, USA). To characterize their macro mechanical properties, Young's modulus and hardness of Au films were measured using the

[z] E-mail: zhuxiaoli@ime.ac.cn

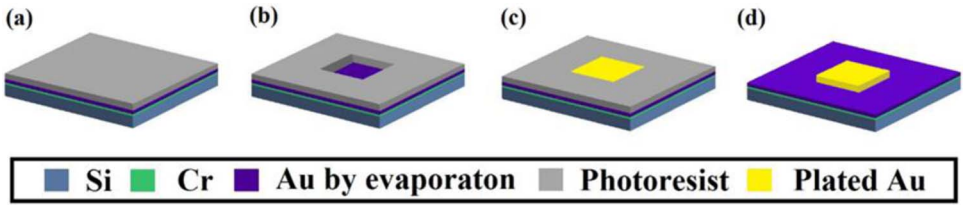

Figure 1. Microfabrication process for electrochemically depositing Au films in sulfite electrolyte.

Agilent Nano Indenter G200 (Agilent Technologies, USA) with a Berkovich indenter and continuous stiffness measurement.

Results and Discussion

Au seed layer.—Figure 2 shows the crystallographic morphology of Au seed layer, presenting the sub-10-nm-resolution orientation maps of Au grains in crystal directions parallel and perpendicular to the film growth, and the grain size distribution. The experiment setup in TKD is shown in Figure 2a. A sample of 20 nm thick Au film with 5 nm Ti adhesion layer deposited on the 5 nm thick Si_3N_4 substrate was put into the vacuum chamber for TKD characterization. To evaluate the resolution in TKD, a Monte Carlo simulation was performed to simulate the trajectories of electrons with a beam size of 1 nm and an accelerating voltage of 30 kV, indicating a high lateral resolution of less than 10 nm (Figure 2c). It can be seen from Figure 2d that more than 97.9% of the indexed grains are oriented with less than 10% deviation from the (111) planes parallel to the film growth orientation. Figure 2e shows the in-plane orientation of the grains which are uniformly distributed between the <101> and <112> orientations which are perpendicular to the (111) planes. From the statistics in Figure 2f, the grain size distribution was obtained by combining the data of all TKD maps achieved on this sample. The average grain size is 44.4 nm and was determined with a standard deviation of 15.5 nm. Therefore, on the seed layer the Au film is polycrystalline and Au grains are preferentially <111> oriented due to that the growth of Au crystals obeys the principle of minimum surface energy.[24,25] This orientation mapping of Au seed layer provides sufficient information including morphology and crystallography of Au seed layer on which Au electrochemical deposition is conducted.

The orientation-controllable growth of Au films.—On polycrystalline Au seed layer, the initial nucleation and the following growth of grains are impacted by many factors in Au electrochemical deposition.[26] Among them, one of the main factors is the applied current density with its corresponding potential, leading to variations in the nucleation and the grain growth in different orientations.[27,28] To investigate the influence of current density on the oriented grain growth in sulfite bath, the different current densities in range of 0.5 mA/cm^2 to 22.2 mA/cm^2 were applied between the anode and the cathodes (i.e. samples). The pulse width and the period were 2 ms and 20 ms, respectively. From XRD spectra shown in Figure 3, it is observed that the intensity of <111> peak increases when current density is in the range of 0.5 mA/cm^2 to 8.9 mA/cm^2, and then

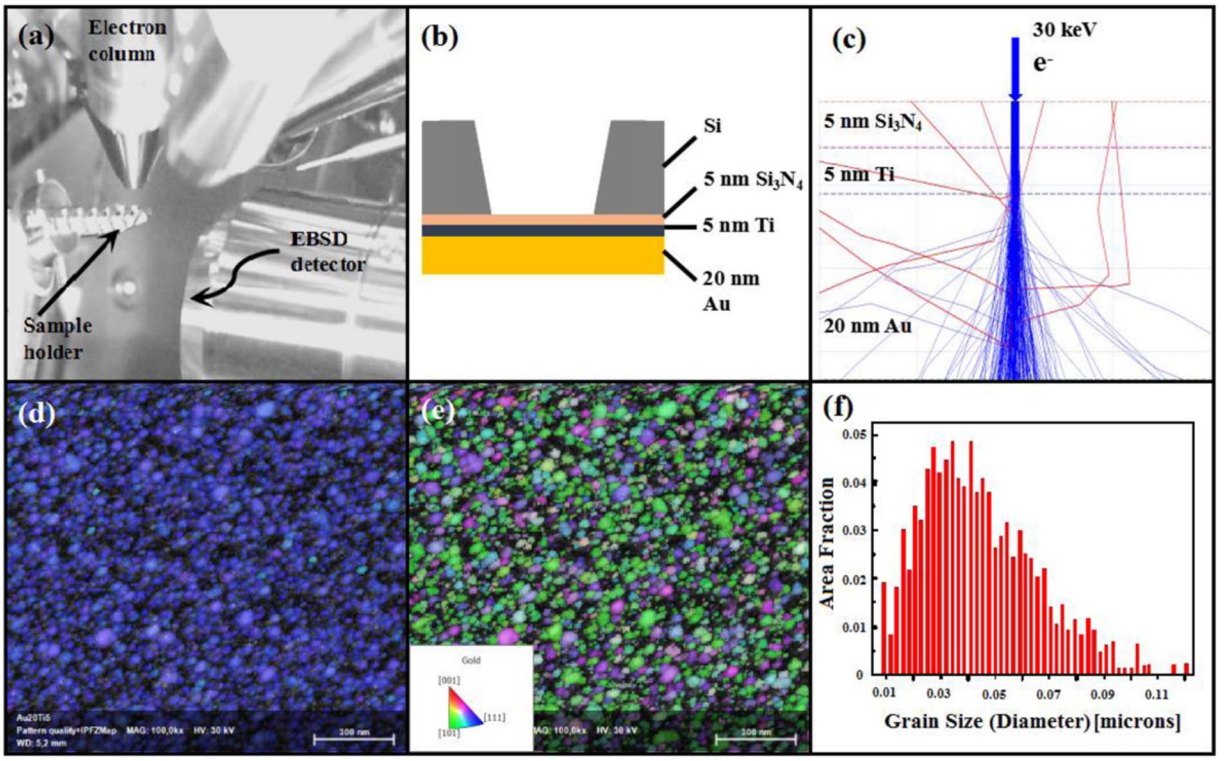

Figure 2. Orientation map revealing the microstructure and crystal orientation of the Au film. (a) In-chamber video camera image of the experimental configuration for TKD analysis; (b) schematic geometry of sample deposited by electron evaporator on 5 nm Si_3N_4 membranes; (c) Monte Carlo simulations (100 000 electrons per simulation) of scattering trajectories for sample and the incident beam with a diameter of 1 nm; (d) inverse pole figure (IPF) map overlaid with pattern quality map of the sample normal direction, (e) of the in plane direction; (f) grain size distribution of the film.

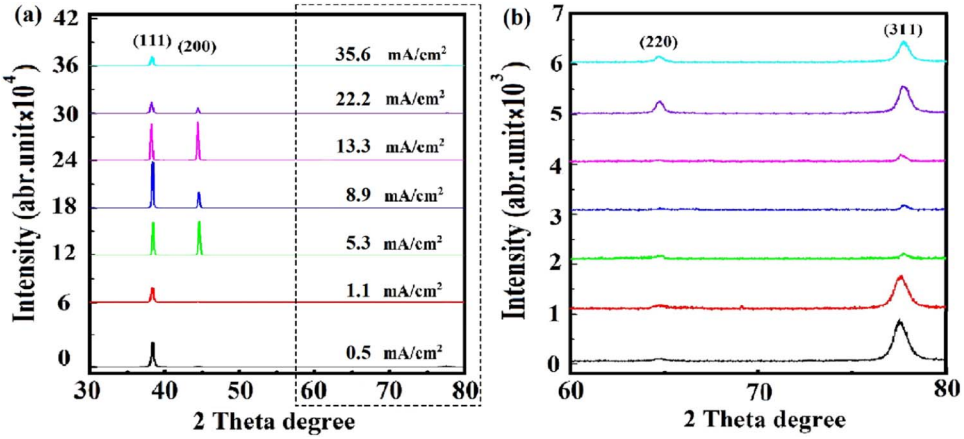

Figure 3. (a) XRD patterns of the Au films deposited at different pulse current densities and (b) zoom-in <220> and <311> peaks.

decreases when the current density becomes larger. In contrast, the variations in trends of <220> and <311> peaks are contrary to the tendency of <111> peak. At the current density of 8.9 mA/cm^2, the XRD spectrum is extremely similar to those taken from single-crystalline Au materials.[29] It implies that, by tuning the pulse current density, grain growth can be controlled mainly at <111> orientation, while the growth at <220> and <311> orientations can be significantly suppressed. In another word, at the current density of 8.9 mA/cm^2, Au films on the surface of cathode grow continuously in the (111) planes. In addition, two strong (200) peaks emerge at the current density of 5.3 mA/cm^2 and 13.3 mA/cm^2, which might be attributed to the growth deviated from (111) planes. It's also worth mentioning that the FWHMs of <111> peaks of samples formed at 5.3 mA/cm^2 and 8.9 mA/cm^2 current densities, are smaller than those of samples achieved at lower or higher current densities, indicative of better crystallinity.

To clarify the impact of pulse current density on the grain growth of Au films, scanning transmission electron microscopy (STEM), selected area electron diffraction (SAED) and high resolution transmission electron microscope (HR-TEM) were used to characterize the cross sections of samples deposited at 0.5 mA/cm^2, 8.9 mA/cm^2 and 22.2 mA/cm^2 current densities (see Figure 4). At low and high current densities (see Figures 4a and 4c), the cross section of samples contain a certain quantity of grains, which average grain sizes are 108.2 nm and 78.2 nm, respectively. Additionally, the difference between these two samples is that the microstructures formed at 22.2 mA/cm^2 current density contains much more nanocrystals on large grains due to higher nucleation rate at high current density. From the SAED patterns in Figures 4d and 4f, the samples formed at the current densities of 0.53 mA/cm^2 and 22.2 mA/cm^2 are typically polycrystalline. In contrast, at the current density of 8.9 mA/cm^2 (see Figure 4b), the cross section of the sample is single crystalline, though contains a certain amount of nanoscale defects and few large crystal structures with orientation perpendicular to the film growth direction. In Figure 4e, the SAED pattern from the selected square area with a width of 200 nm is single crystalline and is also same with those taken from other areas in Figure 4b. It indicates that the achieved film at 8.9 mA/cm^2 is imperfect single crystal, though embedded defects are present. The inserted image in Figure 4h reveals that the measured distance between two planes is 0.235 nm, which corresponds to the distance between (111) planes in the Au face-centered crystal (fcc) structure.[30] In those three cases, the microstructure becomes greatly grainy, single-crystalline, and grainy again with a large amount of fine grains when the applied current density increases from 0.5 mA/cm^2 to 22.2 mA/cm^2. At a medium current density, the single-crystalline Au film can be achieved by electrochemical deposition method.

In Au electrochemical deposition, both the orientation-dependent growth and the microstructures of formed films were experimentally modulated by tuning the applied current density. At different current densities and their corresponding overpotentials, these variations in microstructures and grain sizes originate in the mechanism of film growth including the initial nucleation sites and the following nuclei growth.[31–34] In deposition process, the overpotential provides the energy for nucleation and for grain growth. The larger the overpotential is, the more energy is distributed to the nucleation and grain growth.[35] The rate of nucleation increases with the overpotential based on the equation,

$$v = K_1 \exp(-K_2/\eta)$$

where v is the rate of nucleation, K_1 and K_2 are constant terms, and η is the overpotential. The nucleation rate increases with the applied potential, and so does the nuclei density. The critical radius of Au nucleus also decreases with the increasing overpotential.[36] Regarding the grain growth, the competitive growth at different orientations is affected by the nuclei density and growth rate of grains, both of which are modulated by current densities or overpotentials.

To interpret the impact of pulse current density on the orientated growth and mesocopic texture, hereby exclusive discussions were made to depict the nucleation and grain growth. In terms of the variation of cross sections of Au films (Figure 4), the nucleation and grain growth can be classified into three cases at low, middle and high current densities. In case (a), lower current densities (from 0.5 mA/cm^2 to 1.1 mA/cm^2) result in fewer nuclei and larger average distance between them. In the following pulses, these nuclei continue to grow separately, and thus large grains are formed. Additionally, due to the small amount of gold ions consumption in one pulse period, the diffusion layer might gradually build up. Furthermore, the subsequent nucleation most likely occur around the edges of formed grains, resulting in a deviation of growth from [111] orientation. In case (b), the current densities from 5.3 mA/cm^2 to 8.9 mA/cm^2 lead to the gold atoms grow successively and regularly in (111) planes, resulting in single-crystalline films. However, it is undeniable that some defects are embedded in the single crystals (Figure 4b), which might be attributed to gold grains deviated from (111) plane and some impurities absorbed from electrolyte during deposition. In case (c), when the current density is in the range of 13.3 mA/cm^2 to 35.7 mA/cm^2, more Au nuclei are formed and the growth rate of grains is also greatly enhanced, resulting in larger grain size and squeezing of adjacent growing grains. Therefore, the adjacent growing grains will push each other, and thus overlap other grains around them, leading to the grain growth at other orientations such as <220> and <311> orientations.[37,38]

Morphologies of Au films.—Due to the variations in mechanism of grain growth, the morphologies of Au films significantly vary with different applied current densities. Figure 5 shows the changes in surface roughness of Au films electrochemically deposited using different current densities. It can be seen that, by tuning the current density, the roughness values decreases from 8.7 nm to 3.7 nm, and

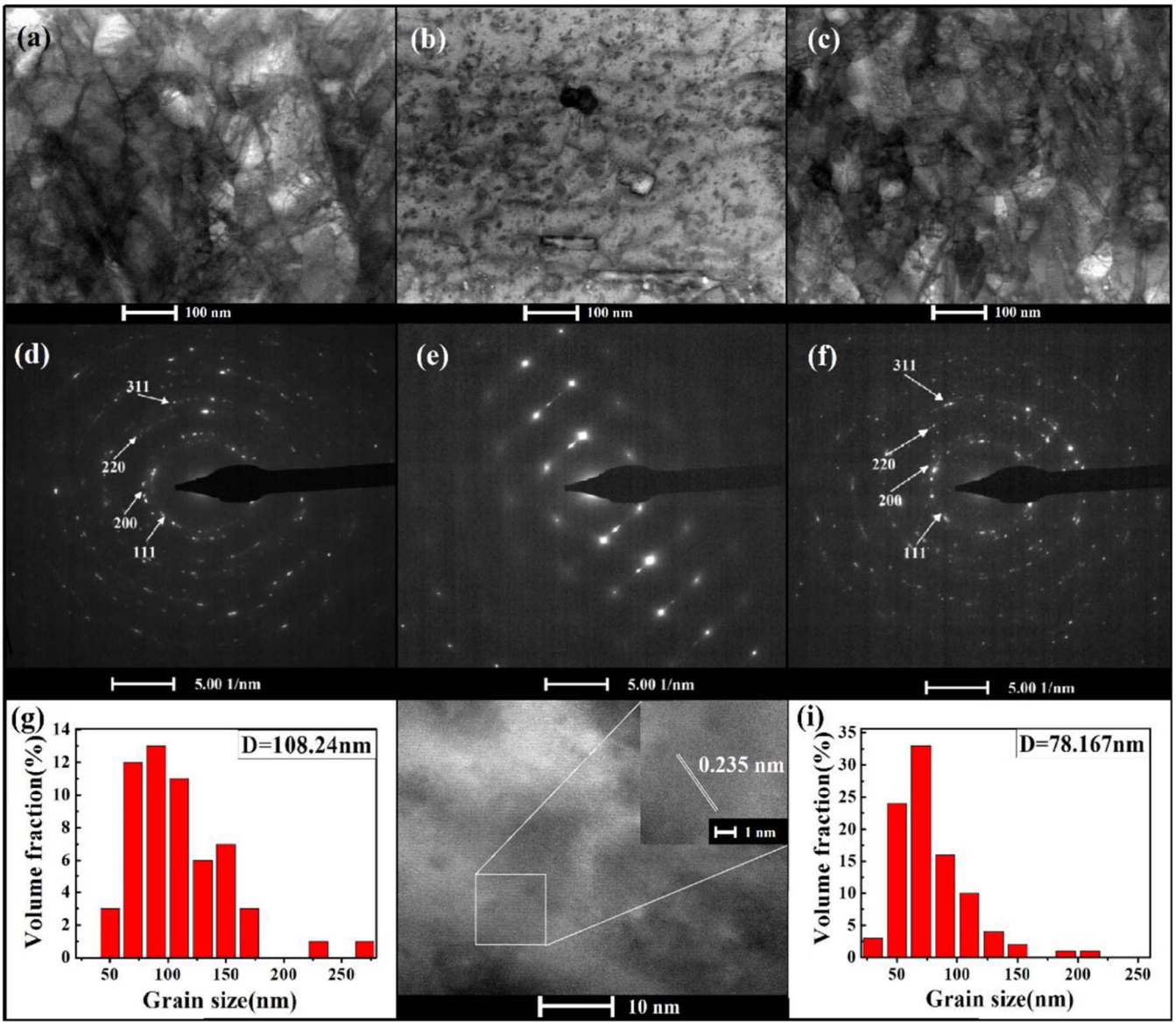

Figure 4. TEM images of Au films deposited at different pulse current densities of (a) 0.5 mA/cm^2, (b) 8.9 mA/cm^2 and (c) 22.2 mA/cm^2, and the corresponding electron diffraction patterns of samples formed at (d) 0.5 mA/cm^2, (e) 8.9 mA/cm^2 and (f) 22.2 mA/cm^2 current densities, respectively; (g) and (i) are the grain size distributions at 0.5 mA/cm^2 and 22.2 mA/cm^2, respectively; (h) The HR-TEM picture of the Au film at 8.9 mA/cm^2 and the zoom-in top-right inserted micrograph shows the 0.235 nm interplanar distance of the (111) planes, for Au fcc structure.

then increases from 3.7 nm to 9.7 nm. When the current density is in range of 0.5 mA/cm^2 to 1.1 mA/cm^2, the rough surface originates in the formation of large grains as shown in Figure 4a. While the current densities from 5.3 mA/cm^2 to 8.9 mA/cm^2 are applied, the smooth surface is achieved resulted from single crystalline of successive growth as shown in Figure 4b. At large current densities of 22.2 mA/cm^2 to 35.6 mA/cm^2, the surface becomes rough again due to the squeezing of fast growing adjacent grains as shown in Figure 4c. The increase of the cathodic current reflects the morphological instability as the dendrites escape the diffusion layer and benefit from spherical diffusion.[39] The roughness of 3.7 nm was achieved at the current density of 8.9 mA/cm^2. It implies that, in Au electrochemical deposition, the current density significantly impact the surface roughness of deposited Au films. As a consequence, a smooth surface can be formed at a medium current density when Au atoms mainly grow in (111) planes.

The mechanical properties of Au films.—The mechanical properties of electrochemically deposited Au films also vary with pulse current density due to their mesoscopic structures. The hardness and Young's modulus of samples achieved at current density rang of 0.5 mA/cm^2 to 22.2 mA/cm^2 were measured using nanoindentation method. To avoid the influence of substrate on the indentation results, the maximum indentation depth was set as less than 500 nm for each indent. Figure 6 presents the trends in the hardness and the Young's modulus of the samples. When the applied current densities are 0.5 mA/cm^2 and 22.2 mA/cm^2, the hardness values of the samples are 2.4 GPa and 1.9 GPa, respectively. The samples are polycrystalline and the grain sizes are 108.2 nm and 78.2 nm, as shown in Figures 4a and 4c, respectively. By contrast, when the current densities are in range of 1.1 mA/cm^2 to 13.3 mA/cm^2, the hardness of chemically deposited films is kept in range of 1.2 GPa to 1.5 GPa. From Figure 4b, the cross section is single-crystalline, though there are fine defects as dislocations embedded in the film. One may argue that the decrease in hardness of samples deposited in current density range of 1.1 mA/cm^2 to 13.3 mA/cm^2 is due to the lack of grain boundaries in the microstructure, leading to the softening of grain boundaries.[40,41]

The Young's modulus of the deposited Au films exhibits a different trend compared with that in hardness. The Young's modulus of Au

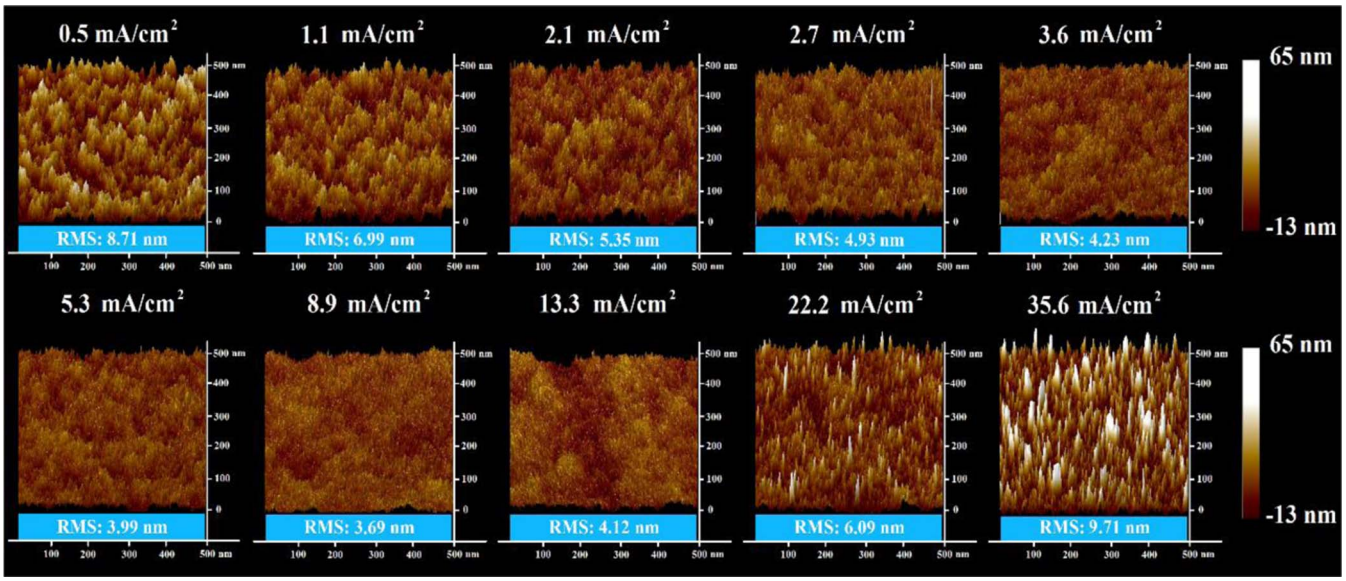

Figure 5. Changes in surface roughness with pulse current densities. AFM micrographs of Au films deposited at different pulse current densities, the roughness of samples were measured using AFM. The scanning area is 500 nm × 500 nm. The minimum surface roughness (Ra) at 8.9 mA/cm^2 is 3.7 nm.

films slightly increase from 103.6 GPa at 0.5 mA/cm^2 to 111.2 GPa at 5.3 mA/cm^2, and subsequently decrease to 104.8 GPa at 22.2 mA/cm^2, still larger than that of standard Au (79 GPa).[42] It implies that the Au films deposited at different current densities have almost same Young's modulus due to the intrinsic properties of Au material.

Conclusions

The orientation of Au film growth was controlled via the modulation of nucleation and growth of nuclei in sulfite plating bath by tuning applied pulse current density. Prior to Au electrochemical deposition, the high-resolution crystallographic morphology of the 20 nm thick Au seed layer is obtained, showing that the Au cathode is polycrystalline and <111> oriented at growth direction, and the grain size is 44.4 nm (± 15 nm). On this cathode, by changing the applied current densities, the growth of Au gains at <111> direction is greatly enhanced and those at other directions are suppressed, leading to a controllable and <111> oriented growth of Au film. The TEM characterization of deposited Au films shows a transition of microstructure from polycrystal at both low and high current densities to imperfect single crystal at the middle ones. Meanwhile, the surface roughness is as low as 3.7 nm at the current density of 8.9 mA/cm^2. The experimental modulation of Au electrochemical deposition using current density can be interpreted by the variation of microstructures. At the current density of 8.9 mA/cm^2, a single-crystalline Au film can be achieved with smooth surface, low hardness and large Young's modulus due to its distinct microstructure. This work reveals that it is possible to control the preferential orientation of the film in environmental-friendly and non-toxic sulfite gold plating bath. This work has also shed light on the insight of kinetics of Au electrochemical deposition in sulfite electrolyte, and would benefit its wide applications.

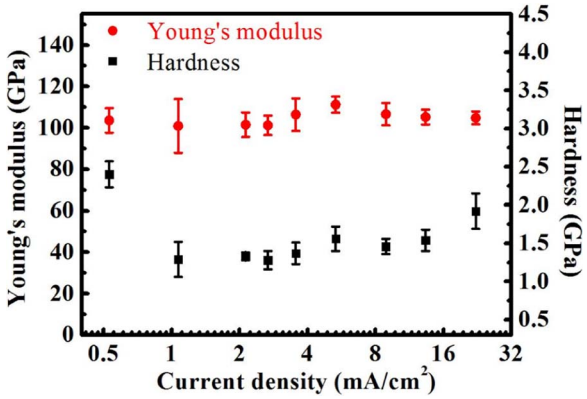

Figure 6. The hardness and Young's modulus of electrochemically deposited Au films.

Acknowledgments

This work was supported by the National Key Research and Development Program of China (2017YFA0206003), National Natural Science Foundation of China (61774166, 61504001), NSFC-RFBR International cooperation and exchange program (NSFC grant No.81811530114, RFBR grant No. 18-52-52010). The authors would like to extend their gratitude to Prof. Mikhail Baklanov for his suggestions.

ORCID

Xiaoli Zhu https://orcid.org/0000-0002-8625-8234

References

1. S. Vallejos, T. Stoycheva, P. Umek, C. Navio, R. Snyders, C. Bittencourt, E. Llobet, C. Blackman, S. Moniz, and X. Correig, *Chem. Commun.*, **47**, 565 (2010).
2. M. D. Kelzenberg, D. B. Turner-Evans, B. M. Kayes, M. A. Filler, M. C. Putnam, N. S. Lewis, and H. A. Atwater, *Nano Lett.*, **8**, 710 (2008).
3. S. Gao, Z. Chen, A. Hu, M. Li, and K. Qian, *J. Mater. Process. Technol.*, **214**, 326 (2014).
4. Z. Liu, M. Zheng, R. D. Hilty, and A. C. West, *Electrochim. Acta*, **56**, 2546 (2011).
5. S. W. Han, H. W. Lee, H. J. Lee, J. Y. Kim, J. H. Kim, C. S. Oh, and S. H. Choa, *Curr. Appl. Phys.*, **6**, E81 (2006).
6. F. Bernhard, S. M. Röhrl, B. Berte, and N. Lars, *Acta Orthop.*, **87**, 42 (2016).
7. M. Schneider, H. Möhwald, and S. Akari, *J. Adhes.*, **79**, 597 (2003).
8. S. Cherevko, N. Kulyk, and C. H. Chuang, *Nanoscale*, **4**, 103 (2012).
9. H. Watanabe, S. Hayashi, and H. Honma, *J. Electrochem. Soc.*, **146**, 574 (1999).
10. M. R. Barati, A. M. Zenkour, and H. Shahverdi, *Compos. Struct.*, **141**, 203 (2016).
11. Y. S. Huang, C. M. Liu, W. L. Chiu, and C. Chen, *Scripta Mater.*, **89**, 5 (2014).
12. A. Ul-Hamid, H. Dafalla, A. Quddus, H. Saricimen, and L. M. Al-Hadhrami, *Appl. Surf. Sci.*, **257**, 9251 (2011).
13. D. Josell, I. Levin, and T. P. Moffat, *J. Electrochem. Soc.*, **162**, D354 (2015).
14. T. Osaka, A. Kodera, T. Misato, T. Homma, Y. Okinaka, and O. Yoshioka, *J. Electrochem. Soc.*, **144**, 3462 (1997).
15. M. Kato and Y. Okinaka, *Gold Bull.*, **37**, 37 (2004).

16. V. I. Kichigin, I. V. Petukhov, D. I. Shevtsov, and M. A. Permyakova, *Russ. J. Appl. Chem.*, **88**, 1950 (2015).
17. D. Liang, J. Liu, K. Reuter, B. Baker-O'Neal, and Q. Huang, *J. Electrochem. Soc.*, **161**, D301 (2014).
18. B. Li, N. Li, G. Luo, and D. Tian, *Surf. Coat. Technol.*, **302**, D202 (2016).
19. D. Josell and T. P. Moffat, *J. Electrochem. Soc.*, **163**, D322 (2016).
20. N. E. Singh-Miller and N. Marzari, *Phys. Rev. B: Condens. Matter*, **80**, 308 (2009).
21. I. Galanakis, G. Bihlmayer, V. Bellini, N. Papanikolaou, R. Zeller, S. Blügel, and P. H. Dederichs, *Europhys. Lett.*, **58**, 751 (2002).
22. S. A. Jang, H. J. Lee, C. V. Thompson, C. A. Ross, and Y. J. Oh, *APL Mater.*, **3**, 126103 (2015).
23. M. A. Khan, P. W. Trimby, H. W. Liu, and R. K. Zheng, *Mater. Sci. Semicond. Process.*, **63**, 237 (2017).
24. M. Todeschini, A. Bastos da Silva Fanta, F. Jensen, J. B. Wagner, and A. Han, *ACS Appl. Mater. Interfaces*, **9**, 37374 (2017).
25. Y. Lee, S. K. Ahn, and Y. Roh, *Surf. Coat. Technol.*, **193**, 137 (2005).
26. G. Holmbom and B. E. Jacobson, *J. Electrochem. Soc.*, **135**, 2720 (1988).
27. H. Tang, CY. Chen, TFM. Chang, T. Nagoshi, D. Yamane, T. Konishi, K. Machida, K. Masu, and M. Sone, *J. Electrochem. Soc.*, **165**, D58 (2018).
28. W. Tang, Y. Hu, and S. Huang, *Met. Mater. Int.*, **18**, 177 (2012).
29. G. Geng, P. Chen, B. Guan, Y. Liu, C. Yang, N. Wang, and M. Liu, *RSC Adv.*, **7**, 51838 (2017).
30. F. Meng, S. F. Bauer, Y. Liao, and I. Baker, *Intermetallics*, **56**, 28 (2015).
31. Y. Zhong, D. Ping, X. Song, and F. Yin, *J. Alloys Compd.*, **476**, 113 (2009).
32. F. Md. Salleh, A. K. Yahya, M. H. Jumali, and Z. Awang, *J. Mater. Sci. Mater. Electron.*, **18**, 843 (2007).
33. S. J. Zheng, K. Du, and X. L. Ma, *J. Eur. Ceram. Soc.*, **28**, 1821 (2008).
34. B. Li, N. Li, G. Luo, and D. Tian, *Surf. Coat. Technol.*, **302**, 202 (2016).
35. J. W. Lee and J. H. Koh, *Ceram. Int.*, **41**, 10442 (2015).
36. X. Peng, J. Wickham, and A. P. Alivisatos, *J. Am. Chem. Soc.*, **120**, 5343 (1998).
37. L. Jacobson and V. Molinero, *J. Am. Chem. Soc.*, **132**, 11806 (2010).
38. M. Sun, C. Zhang, C. Ying, S. Qi, Y. Su, and J. Tian, *J. Mod. Opt.*, **57**, 1598 (2010).
39. E. Sandnes, M. E. Williams, U. Bertocci, M. D. Vaudin, and G. R. Stafford, *Electrochim. Acta*, **52**, 6221 (2007).
40. M. K. Cho, J. W. Cho, J. H. Wu, J. U. Cho, Y. J. Choi, and Y. K. Kim, *Curr. Appl. Phys.*, **10**, 57 (2010).
41. C. E. Carlton and P. J. Ferreira, *Acta Mater.*, **55**, 3749 (2007).
42. B. Wu, A. Heidelberg, and J. J. Boland, *Nat. Mater.*, **4**, 525 (2005).